Formation and Stability of String Phase in Polyamide 6/Polystyrene Blends in Confined Flow: Effects of Nanoparticles and Blend Ratio

Miqiu Kong
Department of Aerospace Material Science and Technology, School of Aeronautics and Astronautics, Sichuan University, Chengdu 610065, P.R. China

Yajiang Huang, Yadong Lv, Qi Yang, and Guangxian Li
Department of Polymer Material Processing Engineering, College of Polymer Science and Engineering, State Key Laboratory of Polymer Materials Engineering of China, Sichuan University, Chengdu 610065, P.R. China

DOI 10.1002/aic.15058
Published online October 2, 2015 in Wiley Online Library (wileyonlinelibrary.com)

Influences of silica nanoparticles on the microstructural evolution of polyamide 6 (PA6)/polystyrene (PS) blends with varying blend ratios were investigated in confined shear flow. Hydrophilic silica nanoparticles were found to promote the formation of PA6 strings with excellent shape stability during shearing. It was ascribed to the promoted coalescence of PA6 droplets induced both by the significantly increased droplet viscoelasticity and confinement, and the reduced interfacial tension by adding silica nanoparticles. Additionally, the width and aspect ratio of droplets obtained by experiments were compared with the predictions of Maffettone–Minale, Minale, Shapira-Haber, MMSH, and modified M models. Good agreements were found in the droplet width in blends with low nanoparticle concentrations, whereas the experimental aspect ratio showed a negative deviation to model predictions, which was attributed to the enhanced droplet viscoelasticity and the omitted droplet orientation angle in these models. © 2015 American Institute of Chemical Engineers *AIChE J*, 62: 564–573, 2016

Keywords: immiscible blend, confined flow, silica nanoparticles, droplet chain, string-like structure

Introduction

In confined geometries, peculiar microstructures are usually exhibited in immiscible blends in flow as compared with the bulk case.[1–4] In confined conditions, at least one dimension of geometries (such as the gap spacing d) is on the micron scale and thus could become comparable to the characteristic size of the dispersed phase (characterized by the droplet diameter $2R$). The morphology evolution in confined condition is not only affected by the material characteristics and the types of flow, but also by the confinement degree (defined as the ratio of the $2R$ to the d, $2R/d$).[5,6] The dynamics of confined droplets are no longer solely governed by the capillary number Ca ($\mathrm{Ca}=\eta_m\dot{\gamma}R/\sigma$, with η_m is the matrix viscosity, $\dot{\gamma}$ the shear rate, and σ the interfacial tension; once the Ca exceeds a critical value, $\mathrm{Ca_{cr}}$, the droplets break up) and viscosity ratio p ($p=\eta_d/\eta_m$, where η_d the droplet viscosity), the effects of the walls also play an important role in the droplet behavior.[1]

The confinement effects could drastically influence the physics of the rheological behavior and morphological evolution of blends during flow. Relevant studies have focused on blends consisting of Newtonian components in confined shear flow.[7,8] Different peculiar structures such as layered structures, pearl necklaces, strings, ribbons, and squashed droplets are observed, depending on the gap spacing d, the blend volume fraction ϕ, and the shear rate $\dot{\gamma}$.[1,5,6,9,10] To gain more insight into the formation of such peculiar morphologies in blends, the dynamics of single confined Newtonian droplets in a Newtonian matrix have been performed. In these Newtonian blends with both component having low viscosity and elasticity, confinement can substantially alter the droplet deformation, orientation, coalescence, and breakup during flow.[11–16] The experimental results are compared with the predictions of the theoretical model, such as the Maffettone–Minale (MM) model,[17] Shapira-Haber (SH) model,[18] Minale (M) model,[19] and MMSH model[20] (Details are shown in the next section). Under rather mild conditions of the shear and the confinement, the theoretical models for confined droplets are relatively successful in describing the shape and the orientation.

Recently, the focus of studies on the dynamics of confined droplets has shifted toward more realistic but hence more complex systems, in which blends contain only one viscoelastic dispersed phase or matrix. It was found that the drop orientation and deformation along the flow direction exhibited a significant increase with both the matrix viscoelasticity and the degree of confinement.[20–22] For instance, in blends with one viscoelastic component, matrix viscoelasticity clearly enhanced the influence of the wall effects on the droplet deformation at a lower $p = 0.45$.[22] Conversely, more complex interactions between confinement conditions and component viscoelasticity on the shape relaxation of fibrils were

Correspondence concerning this article should be addressed to Y. Huang at hyj@scu.edu.cn (or) G. Li at guangxianli@scu.edu.cn.

explored.[23,24] It was shown that viscoelastic droplets are more stabilized by confinement compared with Newtonian droplets[25,26]; matrix viscoelasticity, conversely, induced a destabilization, thereby shifting the Ca_{cr} of confined droplets to smaller values.[26] For example, in systems with either a viscoelastic matrix or droplet in the confined shear flow,[27] the Ca_{cr} of a viscoelastic droplet was found to be similar to a Newtonian one, whereas matrix viscoelasticity caused breakup at a much lower Ca, which affected the breakup mode. Confined viscoelastic droplets in a Newtonian matrix broke up into multiple parts, only two daughter droplets were broken up in a viscoelastic matrix, up to very large $2R/d$.

Nonetheless, real industrial immiscible blends are typically consisting of two viscoelastic components but related studies on blends in confined flow are relatively rare.[28] Son et al.[28] investigated the stability of polyamide 6 (PA6) threads confined in quiescent polystyrene (PS) matrix with $0.33 < 2R/d < 0.77$ and found that an initially axisymmetric thread became nonaxisymmetric, the growth rate of the instabilities decreased, and the wavelength increased as compared with the unconfined situation. Usually, to improve the poor interfacial adhesion of immiscible blends, additives (such as nanoparticles or copolymers) are added.[29–33] So one of the challenge is to predict how the additives affect the morphology development (such as droplet breakup, coalescence, and deformation) in the confined flow.[26,34] For instance, Moldenaers and coworkers[26] found that in the presence of an interfacially active block polymer in Newtonian systems, the breakup of confined droplets was inhibited for the $p=0.4$, and compared with the bulk behavior, the droplet length at the breakup of confined droplets was reduced. Moreover, both the deformation and orientation of polydimethylsiloxane (PDMS) droplets in polyisobutylene (PIB) matrix is suppressed by the addition of the PIB-PDMS block copolymer.[34] It was clear that the interfacial and component modification could significantly alter the dynamics of confined droplets. In recent years, nanoparticles were introduced into blends as a compatibilizer.[29,35] Relevant researches focused on effects of nanoparticles on the morphology development such as the droplet coalescence, breakup, and relaxation behavior in the bulk flow, while in the confined shear flow investigations on industrially relevant blends with viscoelastic components and adding a compatibilizer are scarce.

The purpose of this work is to probe into the effects of silica nanoparticles on the morphology development of immiscible blends consisting of two viscoelastic components in confined shear flow. *In situ* time resolved light microscopy was used to gain insight into the effects of silica nanoparticles on the structural developments of PA6/PS blends with viscoelastic components, in which silica nanoparticles were selectively dispersed in PA6 phase. Influences of droplet concentration (5, 10, and 20 vol %), shear rate (0.1 and 0.3 s^{-1}), and silica nanoparticle content (0, 1, 3, and 5 vol %) on the morphology development are systematically investigated in confined shear flow. Moreover, comparisons of the experimental width and aspect ratio of droplets with the model predictions were made.

Models

The shape of a moderately deformed droplet is generally described by the three axes of the droplet, L, B, W, and the orientation angle, θ, which is the angle between the longest droplet axis L and the flow direction. A schematic representation of a deformed droplet in a simple shear flow is shown in Figure 1.

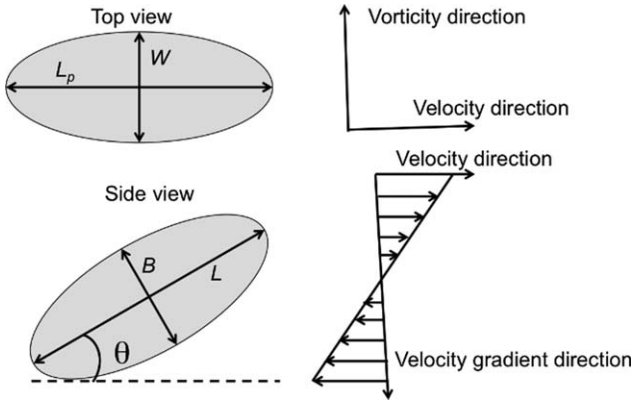

Figure 1. Schematic representation of a deformed droplet with the geometrical parameters in shear flow.

When the droplet deformation in flow is small ($Ca \ll 1$), the deformation parameter, D, is defined as $D = (L - W)/(L + W)$. For highly deformed droplet, a more appropriate deformation parameter is defined as $r_p = L/W = (1+D)/(1-D)$.

Droplet deformation in a bulk shear flow are given by a phenomenological MM model,[17] assuming that the drop is an incompressible ellipsoid during flow. The MM model was suitable for p below and above one, up to Ca_{cr}. For simple shear flow, the droplet deformation D, width W, and orientation angle θ is defined as

$$D_{MM} = \frac{f_{2MM}\mathrm{Ca}}{\sqrt{f_{1MM}^2 + \mathrm{Ca}^2} + \sqrt{f_{1MM}^2 + \left(1 - f_{2MM}^2\right)\mathrm{Ca}^2}} \tag{1}$$

$$W = 2R\left[\frac{f_{1MM}^2 + \mathrm{Ca}^2 - f_{2MM}\mathrm{Ca}\left(f_{1MM}^2 + \mathrm{Ca}^2\right)^{1/2}}{\left(f_{1MM}^2 + \mathrm{Ca}^2\right)^{1/3}\left(f_{1MM}^2 + \mathrm{Ca}^2 - f_{2MM}^2\mathrm{Ca}^2\right)^{2/3}}\right]^{1/2} \tag{2}$$

$$\theta_{MM} = \frac{1}{2}\arctan\left(\frac{f_{1MM}}{\mathrm{Ca}}\right) \tag{3}$$

where f_{1MM} and f_{2MM} are dimensionless functions of Ca and p given by

$$f_{1MM} = \frac{40(p+1)}{(2p+3)(19p+16)},\ f_{2MM} = \frac{5p+3}{2p+3} + \frac{3\mathrm{Ca}^2}{2+6\mathrm{Ca}^2} \tag{4}$$

For droplets confined between two parallel walls, the theory of Shapira and Haber[18] (SH model) adds an additional deformation to the Taylor deformation[36]

$$\begin{aligned} D_{SH} &= D_{Taylor}\left[1 + C_s\frac{1+2.5p}{1+p}\left(\frac{R}{d}\right)^3\right], \\ D_{Taylor} &= \mathrm{Ca}\frac{16+19p}{8(1+p)}\sin\theta\cos\theta \end{aligned} \tag{5}$$

C_s is taken to be equal to 5.699, assuming the droplet is positioned symmetrically between the two confining walls.[18] D_{Taylor} is the deformation parameter from the small-deformation bulk theory of Taylor,[36,37] in which $\theta = \pi/4$. This model is only applicable for small $2R/d$. The droplet shape remains ellipsoidal and unaltered with respect to the Taylor small-deformation prediction and p around unity for the bulk flow. To extend the applicability of SH model to p different from 1 and large deformations, Vananroye et al.[20] proposed to replace the Taylor bulk deformation parameter D_{Taylor} with steady-state deformation expression D_{MM} of the Maffettone

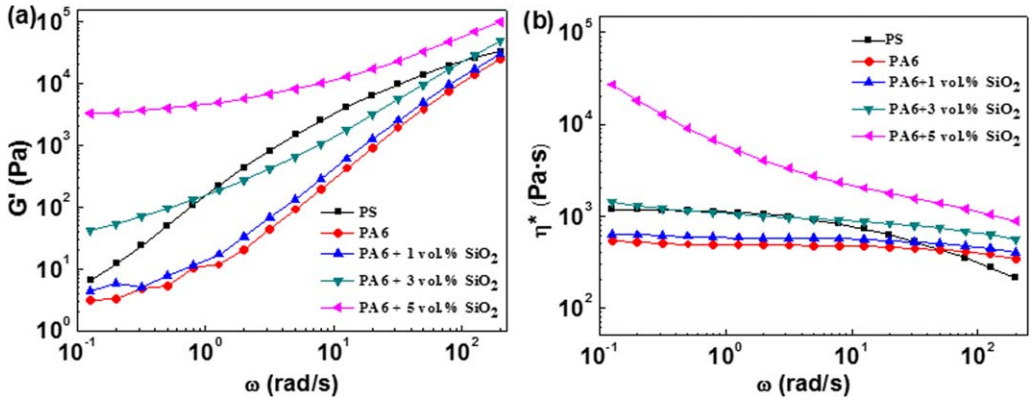

Figure 2. (a) Storage modulus (G') and (b) complex viscosity (η^*) as a function of frequency (ω) for PS and PA6 composites filled with different volume fractions of SiO_2 nanoparticles at 230°C.

[Color figure can be viewed in the online issue, which is available at wileyonlinelibrary.com.]

and Minale model,[17] leading to a combined MMSH model with deformation parameter D_{MMSH}

$$D_{MMSH}=D_{MM}\left[1+C_s\frac{1+2.5p}{1+p}\left(\frac{R}{d}\right)^3\right] \tag{6}$$

with D_{MM} is an expression for the droplet deformation parameter in MM model. In this approach, the dependence on the orientation angle disappears.

Minale[19] modified the MM model to a generic confined flow, referred as M model, by proposing expressions for f_{1M} and f_{2M}, consisting of the parameters f_{1MM} and f_{2MM} in the MM model, are corrected with a confinement factor $(R/d)^3$

$$f_{1M}=\frac{f_{1MM}}{1+C_s\left(\frac{R}{d}\right)^3 f_{1c}},\ f_{2M}=f_{2MM}\left[1+C_s\left(\frac{R}{d}\right)^3 f_{1c}\right] \tag{7}$$

The term R/d in the expression of f_{1M} and f_{2M} accounts for the degree of confinement, and the functions f_{1c} and f_{2c} are defined as follows

$$f_{1c}=\frac{44+64p-13p^2}{2(1+p)(12+p)},\ f_{2c}=-\frac{10-9p}{12+p} \tag{8}$$

The M model is introduced an effective viscosity to make the model more suitable for realistic blends.[5] The effective viscosity is taken according to Choi and Showalter[38]

$$\eta_{mef,f}=\eta_m\left[1+\phi\frac{5p+2}{2(p+1)}\left(1+\phi\frac{5(5p+2)}{4(p+10)}\right)\right] \tag{9}$$

where ϕ is the blend volume fraction. This changes the Ca and the p in the M model. This model is referred as the modified M model (mM model).

Experimental

Materials

The PA6 (YH800, Yueyang petrochemical Co.,) has a density of 1.14 g/cm^3 and a melting point of 215–220°C. The PS (GP5250, Taihua Plastic (Ningbo) Co.,) has a density of 1.05 g/cm^3 and a melt flow index (MFI) of 7.0 g/10 min. The hydrophilic fumed silica (Aerosil A200, Degussa Corp.) with a specific surface area of 200 m^2/g, a density of 2.3 g/cm^3, and an average diameter of 12 nm was used. The PA6 was precompounded with various amounts of silica nanoparticles (0, 1, 3, and 5 vol %). Then the obtained PA6/SiO_2 composites were dispersed within the PS matrix via a second extrusion step to obtain the blends. The processing conditions and the sample preparation of all blends and composites could be found in our previous paper.[39]

The viscoelastic properties of polymer components were measured using a strain-controlled rheometer ARES (TA Instrument) under nitrogen atmosphere in our previous paper.[39] Figure 2 showed the dependence of the storage modulus (G') and complex viscosity (η^*) as a function of frequency (ω) for PS and PA6 composites filled with different volume fractions of silica nanoparticles at 230°C. It was showed that the viscoelasticity of PA6 was notably enhanced on the addition of 3 and 5 vol % silica nanoparticles. For the 5 vol % silica nanoparticle filled PA6, an obvious yield stress behavior can be detected at low frequencies. Zero-shear viscosities of the PS, PA6, and PA6/SiO_2, and the interfacial tension of the blends at 230°C were reported in Table 1. The viscosity ratio, p, and the critical capillary number, $Ca_{cr}(p)$ calculated by de Bruijin's equation[40] for our blends were also showed in Table 1. Table 1 also showed that the interfacial tension of PA6/PS blends was decreased with the addition of silica nanoparticles. It was because that although hydrophilic silica nanoparticles mainly located within the PA6 dispersed phase, there were still a small portion of them on the surface of PA6 dispersed phase.[41]

Methods

Flow visualization experiments in confined condition were performed in a Linkam shear cell (CSS-450 from Linkam Scientific Instruments, UK), consisting of two parallel quartz plates. The bottom plate is connected to a dynamic motor, and the gap width between the plates is adjusted by a stepper motor and was consistently set to 50 μm in this study. Prior to each experiment, the gap spacing and the parallelism of the plates were carefully checked by performing transmitted light

Table 1. Rheological Properties and Interfacial Tension of the Systems at 230°C

SiO_2 Contents	η_0^{PA6/SiO_2} (Pa · s)	p	α (mN/m)	Ca_{cr}
0 vol %	666.7	0.61	7.4	0.46
1 vol %	684.9	0.63	5.8	0.46
3 vol %	2046.2	1.87	5.6	0.65
5 vol %	18,638.2	17.0	5.4	–

The zero-shear viscosity of PS (η_0^{PS}) is 1095 Pa·s.

Table 2. Compositions of the (PA6/SiO_2)/PS Blends Used in this Study

(PA6/SiO_2)/PS	5/95	10/90	20/80
0 vol % SiO_2	A5	A10	A 20
1 vol % SiO_2	A5-1	A10-1	A20-1
3 vol % SiO_2	A5-3	A10-3	A20-3
5 vol % SiO_2	A5-5	A10-5	A20-5

All used the volume fraction.

intensity measurements on colored solutions at different gaps.[10] Using this procedure, the gap setting has an accuracy of ± 5 μm. Microscopic observations are made by placing the cell on an optical microscopy stage. An optical microscope (Olympus BX51, Japan) is used to detect the morphology development during shear flow and after the cessation of the flow. All images are acquired in the velocity-vorticity plane with a PixelLINK CCD camera and analyzed using image analysis software (commercial Linksys32 DV video software).

After the sample was loaded into the shear cell and the temperature remained at 230°C, the sample was sheared at 0.1 s^{-1} for 20,000 s and then the shear rate was increased abruptly to 0.3 s^{-1} for another 20,000 s. It was found that shearing for 2000–6000 strain units was adequate for the blends to reach their steady-state morphology. From the microscopy images obtained, the axis L_p in the velocity direction and the width W perpendicular to the velocity direction could be determined directly. Three compositions (5, 10, and 20 vol % of PA6/SiO_2 composites) showed in Table 2 were chosen to study the influence of silica nanoparticle concentration and dispersed phase concentration on the morphology evolution of blends in the confined flow.

Results and Discussion

Effect of silica nanoparticles

Figure 3 showed the morphology evolution of the (PA6/SiO_2)/PS 5/95 (A5) blends filled with different concentrations of silica nanoparticles in confined shear flow. The initial droplet size of the pure A5 blend is about 7.3 μm (the confinement ratio is $2R/d = 0.15$), as shown in Figure 3a. With the selective distribution of silica nanoparticles in the PA6 dispersed phase, the initial morphology of A5-1 and A5-3 blends in this condition was refined significantly (Figures 3e, i) while a coarsened morphology was observed in the A5-5 blend (Figure 3m). This morphology variation observed was ascribed to the enhanced viscoelasticity and declined interfacial tension on the addition of silica nanoparticles.[41] It makes the confinement degree of droplets ($2R/d$) decreased in the A5-1 and A5-3 blends but increased in the A5-5 blend. When shearing at 0.1 s^{-1}, the filled PA6 droplet coalescence in PS matrix occurred, resulting in increasing the droplet confinement. Owing to the wall migration effect,[9] the droplets of A5, A5-1, and A5-3 blends developed from a randomly distributed and multilayered droplets to regularly arranged droplet chains displayed as a single-layer, the large droplets self-organize into pearl necklace structure (Figures 3b, f, and j). In the A5-5 blend, the large droplets also self-organized into pearl necklace structures or strings after shearing at 0.1 s^{-1} (Figure 3n). It can be seen that

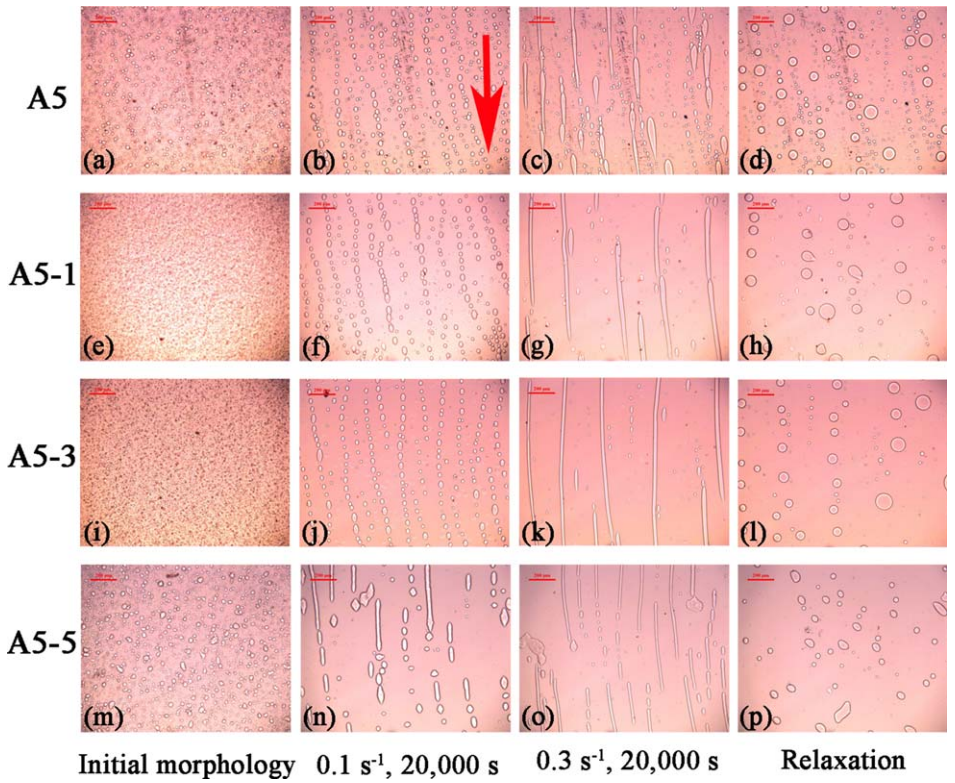

Figure 3. Morphology of (PA6/SiO_2)/PS 5/95 blends filled with hydrophilic silica at 230°C at $d = 50$ μm before shearing (the first column), after shearing at 0.1 s^{-1} for 20,000 s (the second column), then shearing at 0.3 s^{-1} for another 20,000 s (the third column), and after relaxation for 204 s (d), 313 s (h), 496 s (l), and 4771 s (p) (the last column).

The red arrow denotes the flow direction, and the scale bar represents 200 μm. [Color figure can be viewed in the online issue, which is available at wileyonlinelibrary.com.]

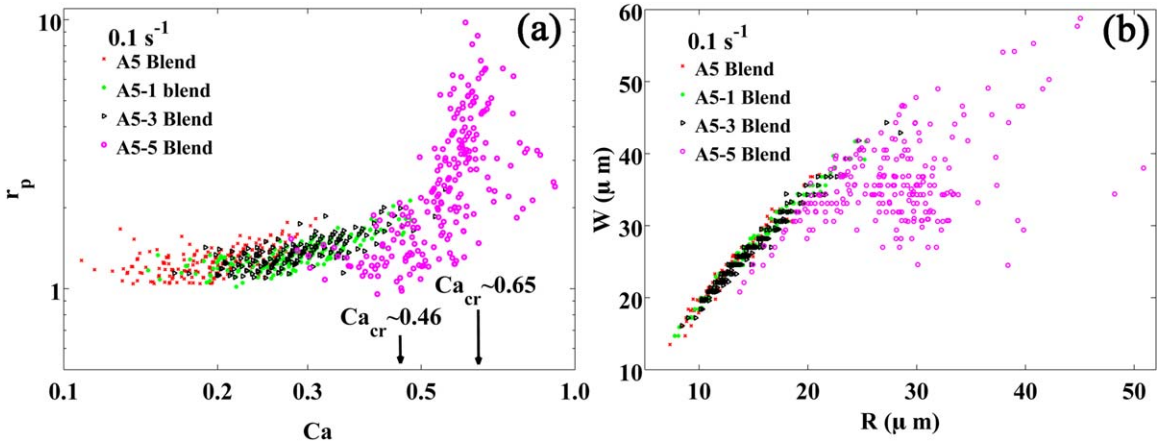

Figure 4. (a) Experimental droplet aspect ratio (r_p) vs capillary number (Ca); (b) Experimental steady-state droplet widths (W) as a function of their equivalent radius (R).

Experimental data measured from microscopy images of A5 blends filled with silica nanoparticles at 0.1 s^{-1} for 20,000 s and $d = 50$ μm. [Color figure can be viewed in the online issue, which is available at wileyonlinelibrary.com.]

the formation of regular droplet chains in confined shear flow was promoted by adding silica nanoparticles although the initial confinement degree was decreased.

With increasing the shear rate up to 0.3 s^{-1}, the droplet-string transition of PA6 phase was observed. Figure 3c depicted that a single-layer consisting of long elongated droplet chains and pearl necklaces of droplets emerged in the pure A5 blend. However, regularly arranged chains coalesced further into long strings in A5-1, A5-3, and A5-5 blends, as shown in Figures 3g, k, and o. The droplet-to-string transition was reported to proceed via the coalescence of droplets in four stages by Migler,[1] namely the coalescence of nearby droplets, the self-organization of larger droplets into pearl necklace structures, the formation of strings, and the formation of widen ribbons (where $W > d$). It was found that the first three steps were observed in the process of morphology development of the filled A5 blend while the ribbon-like structure was absent. With the increase of nanoparticle content, the formed strings then coalesced with each other and displayed longer strings. The formation of regular droplet chains may be related to the viscoelastic normal stresses of the components, which resulted in an attractive interaction between the droplets moving under the shear flow.[42] Another possible reason as proposed by Migler,[1] namely the distortion of velocity fields around droplets by the walls in highly confined geometry, cannot be excluded because it can also produce enhanced attractive interaction between droplets. In this case, the introduction of silica nanoparticles can enhance the viscoelasticity of filled PA6 phase and reduce the interfacial tension of filled blends (Table 1 and Figure 2), which facilitated the formation of strings in the filled blends.

After the stop of shearing, the confined droplets were allowed to relax into their steady shape, as shown in Figures 3d, h, l, and p, and we defined this period of time as the relaxation time (τ) from now on. For A5, A5-1, and A5-3 blends, the droplets broke up and then retracted back to spherical shape, and correspondingly the τ was about 204 s, 313 s, and 496 s, respectively. Note that although the droplets in the A5-5 blend broke up into smaller droplets, these small droplets were unable to retract into spherical droplets even after relaxation for nearly 4800 s possibly due to their significantly enhanced viscoelasticity as shown in Figure 2. This meant that the relaxation of filled droplets in confined conditions became slower when the nanoparticle concentration increased. Our previous study[39] has shown that the relaxation time of PA6 droplets filled with 0, 1, 3, and 5 vol % silica nanoparticles in PS matrix (a bulk-like morphology, $d = 1600$ μm) was approximately 270 s (AR = 10.8, AR is the aspect ratio of the droplet and is defined as the ratio of the length L to the diameter D of the droplet), 470 s (AR = 11.5), 540 s (AR = 14.0), and 3,515 s (AR = 23.2), respectively (the droplet diameter is about 80 μm). The relaxation time of droplets in the confined and bulk behavior can be scaled by their volume conservation, and then it can be seen that the relaxation time of droplets in confined condition is longer than that in the bulk condition. The previous work[39] indicated that the retarded relaxation in the bulk case was the results of the remarkably improved viscoelasticity and reduced interfacial tension. Besides, confinement can suppress the growth of the droplet instability.[7,28] Thus, in this study, the improved stability of the droplets in the confined condition could be attributed to both the significantly enhanced droplet viscoelasticity and reduced interfacial tension induced by silica nanoparticles (Figure 2 and Table 1), and the confinement.

Comparison of steady-state droplet deformation with model prediction

The measured deformation r_p (θ=0) of steady-state droplets for different filled A5 blends after shearing at 0.1 s^{-1} for 20,000 s in the confined geometry was presented in Figure 4a as a function of the corresponding Ca. The r_p was given by $r_p = L_p/W$, where the projected axis L_p of the droplet in the velocity direction was measured assuming θ=0 ($L = L_p$, $B = W$). The r_p was found to be increased with the increase of the Ca, and shifted toward higher Ca values as the concentration of silica nanoparticles increased. Some of the silica nanoparticle filled droplets still stayed stable under flow up to Ca beyond the Ca_{cr} in bulk, as shown in Figure 4a. It suggested that silica nanoparticles can improve the stability of droplets and promote the formation of long strings in confined A5 blends. This promoted formation of strings with improved stability might be ascribed to the enhanced droplet viscoelasticity (Figure 2) and the reduced interfacial tension (Table 1) by adding silica nanoparticles. Figure 4b showed the width W of droplets as a function of their equilibrium radius R at $d = 50$ μm after shearing at 0.1 s^{-1} for 20,000 s. The R of

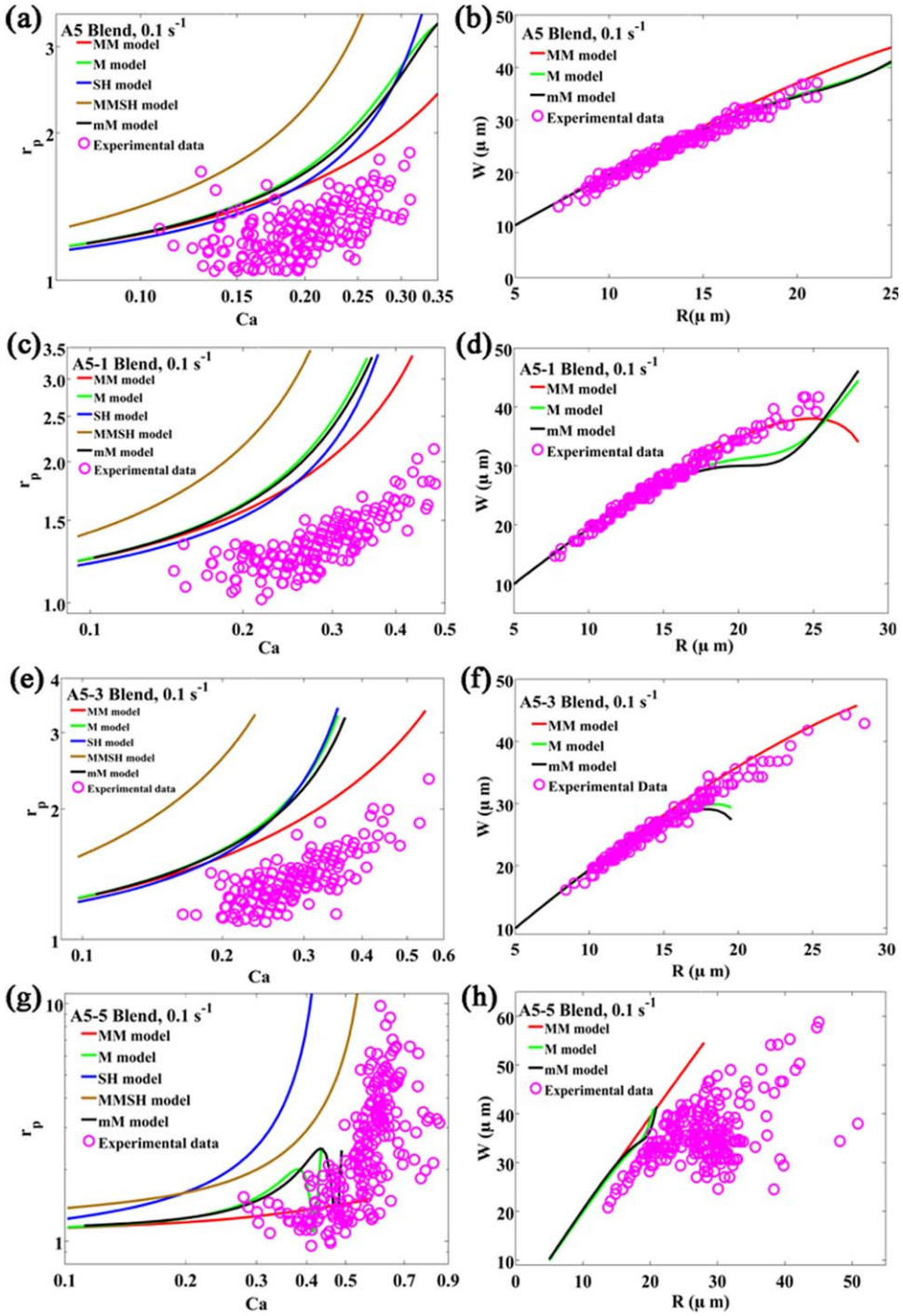

Figure 5. Left: steady-state droplet aspect ratio (r_p) vs capillary number (Ca).

Experimental data measured assuming $\theta = 0$ (symbols), and the lines represent the theoretical r_p predicted by models. Right: steady-state droplet widths (W) as a function of their equivalent radius (R), experimental W (symbols) measured from microscopy images, and lines denote the theoretical W from models. A5 blends with different SiO_2 contents (0, 1, 3, and 5 vol %) shearing at 0.1 s^{-1} for 20,000 s and at $d = 50$ μm. [Color figure can be viewed in the online issue, which is available at wileyonlinelibrary.com.]

droplets was determined by assuming the equivalent volume of deformed ellipsoids or strings and corresponding isotropic sphere or cylinder after the ceasing of shear flow. It was found that for A5 blends with lower contents of silica nanoparticles (0–3 vol %), the W increased almost linearly with the increase of R. In the A5-5 blend, the W of droplets at lower R increased almost linearly with increasing the R while it became very scattered at higher R. Usually, the best dispersion of droplets in blends is obtained when the p is close to unity.[4] As shown in Table 1 and Figure 2, the p of A5 (0.61), A5-1 (0.63), and A5-3 (1.87) blends is approaching unity while the droplet viscoelasticity in the A5-5 blend are significantly enhanced ($p = 17$). This obviously improved droplet viscoelasticity may be responsible for the wide distribution in the r_p and W of droplets in the A5-5 blend.

Figure 5 compared the r_p and W of droplets obtained by experiments for different A5 blends with the theoretical predictions (lines) from the MM, M, SH, MMSH, and mM

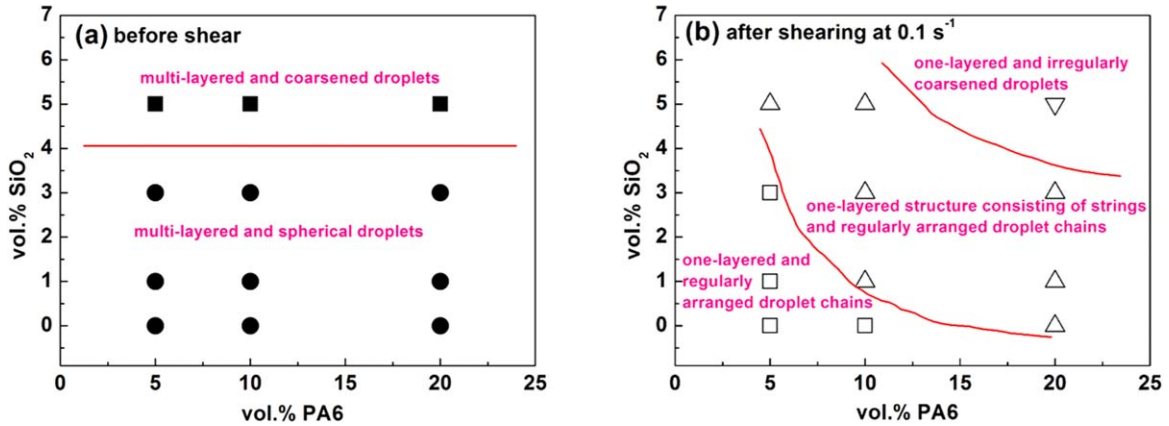

Figure 6. Morphology diagram describing microstructure in confined (PA6/SiO_2)/PS 5/95, 10/90, and 20/80 blends, in which PA6 phase filled with different contents of hydrophilic silica nanoparticles (0, 1, 3, and 5 vol %) before shearing (a) and after shearing at 0.1 s^{-1} for 20,000s (b).

Different symbols for different observed states: (●) multilayered, randomly distributed and spherical droplets, (■) the multilayered, randomly distributed and coarsened droplets, (□) regularly arranged droplet chains/pearl necklace structure, (△) single-layered structure consisting of strings and regularly arranged droplet chains, and (▽) the single-layered and irregularly coarsened droplets. [Color figure can be viewed in the online issue, which is available at wileyonlinelibrary.com.]

models. The experimental r_p of A5, A5-1, and A5-3 blends exhibited a negative deviation to model predictions (Figures 5a, c, and e). For the A5-5 blend (Figure 5g), all models cannot describe its deformation behavior. Similar negative deviations of the experimental r_p from theoretical predictions were found in Newtonian PIB/PDMS blends with 1 wt. % PIB for $Ca \geq Ca_{cr}$, whereas positive deviations were found in this blend with 5 wt. % PIB at low Ca.[10] But Pathak and Migler[6] observed positive deviations from the models for $Ca > Ca_{cr}$. Here, the Ca of the A5 blend at 0.1 s^{-1} is 0.05, below $Ca_{cr} = 0.46$ (Table 1). Nevertheless, the positive deviation of theoretical $r_p \sim Ca$ curves to the experimental data is seen. It might be attributed to the presence of the non-zero orientation angle of droplets in shear flow. Under shear flow, the major axis of droplets determined directly from the projected L_p is smaller than its real value L ($L_p < L$) due to the presence of droplet orientation angle in shear flow. It is seen that the experimental $r_p = L_p/W$ is lower than the model predictions, thereby displaying a negative deviation from the model predictions. The experimental W of droplets in different A5 blends was shown in Figures 5b, d, f, and h. For the A5 blend, the experimental W of droplets can be predicted satisfactorily by all models. In A5-1 and A5-3 blends, the experimental W agreed well with the predictions by the M and mM models at lower R but showed a positive deviation to both model predictions at higher R. It should be noted that all models failed to describe the experimental W of droplets for the A5-5 blend and displayed a positive deviation to the experimental data. This is because that the morphology of the A5-5 blend became coarsened (Figure 3) due to the significantly enhanced droplet viscoelasticity (Figure 2). And the droplets with large size generated higher deformation, then the width of droplets in the A5-5 blend is smaller than the model prediction according to the volume conservation of droplets.

Effect of filled dispersed phase concentration

Figure 6 showed the overall effects of the PA6 phase concentration (5, 10, and 20 vol %) on the morphology evolution of PA6/PS blends in confined shear flow, in which for each PA6 concentration, the PA6 phase was filled with different loadings (0, 1, 3, and 5 vol %) of silica nanoparticles. The morphology diagram is summarized in the parameter space of volume fraction of PA6 phase (vol % PA6) and silica nanoparticles (vol % SiO_2). Figure 6a displayed the initial morphology of blends. For blends free of or filled with low concentrations (1 and 3 vol %) of silica nanoparticles, multilayered, randomly distributed, and spherical droplets were presented (shaded circle points in Figure 6a). For blends filled with 5 vol % silica nanoparticles, multilayered, randomly distributed and coarsened droplets were exhibited (shaded square points in Figure 6a). The variation in the initial morphology of these blends may be related with the changes in viscoelastic and interfacial properties on the introduction of silica nanoparticles as interpreted in our previous paper.[41] After shearing at 0.1s^{-1} for 20,000 s, the morphology of confined blends was demonstrated in Figure 6b. In the blends filled with both the lower concentrations of PA6 phase and the lower loadings of silica nanoparticles, the morphology was developed from a randomly distributed and multilayered droplets to regularly arranged droplet chains or pearl necklace structure displayed as a single-layer during confined shear flow (open square points in Figure 6b). For the blends with moderate concentrations of PA6 phase and lower loadings of silica nanoparticles or lower concentrations of PA6 phase and higher loadings of silica nanoparticles, the morphology changed from a randomly distributed, multilayered and spherical droplets or coarsened and multilayered droplets to the structure consisting of strings and regularly arranged chains in confined shear flow (open triangle points in Figure 6b). For blends with both the highest concentration of PA6 phase and the highest loading of silica nanoparticles, the morphology exhibited single-layered and irregularly coarsened droplets with larger size (open inverted triangle points in Figure 6b).

The morphological transition of blends from multilayered structure to single-layered and arranged droplet chains or necklace structure in confined shear flow could be ascribed to the strong wall migration effect[9] and the attractive interaction between the droplets moving under shear flow induced by the viscoelastic normal stresses of the components.[42] In Figure 6b, it is observed that the shear-induced formation of strings was enhanced in the concentrated pure blend after shearing at 0.1 s^{-1}. This can be understood by the increase both in the

Table 3. The Initial Droplet Diameter (2*R*) and the Capillary Number (Ca) for PA 6/PS Blends with 5, 10, and 20 vol % PA 6 dispersed phase

		Ca	
PA 6/PS	2*R* (μm)	$\dot{\gamma}$=0.1 s^{-1}	7=0.3 s^{-1}
5/95	7.3	0.05	0.16
10/90	10.5	0.08	0.23
20/80	29.5	0.22	0.65

droplet size and number density of droplets at higher PA6 concentrations. It is known that the droplet size in immiscible blends would increase as the droplet concentration increases due to the occurrence of promoted coalescence by the concentrated blends.[43] In the presence of silica nanoparticles, although the initial morphology is refined, the shear-induced formation of strings was also promoted. It may be attributed to the increased droplet confinement by the promoted coalescence of PA6 droplets during shearing due to the enhanced viscoelasticity of the PA6 droplets and reduced interfacial tension of the filled blends (Figure 2 and Table 1).[41]

For pure blends, the initial size (2*R*) of droplets in blends at $d = 50$ μm was given in Table 3. The 2*R* was found to increase from 7.27 μm for the A5 blend ($2R/d = 0.15$), to 10.50 μm and 29.45 μm for the A10 ($2R/d = 0.21$), and A20 blends ($2R/d = 0.59$), respectively. It can be seen that the confinement degree was enhanced with increasing PA6 content. When shearing at 0.1 s^{-1} where the Ca < Ca_{cr} (Table 3), the dynamics of droplets are dominated by coalescence, and the confinement degree of droplets are increased. Thus, more strings were found to form in concentrated blends. As shown in Figure 6b, in the A20 blend, the pearl necklace structure and strings coexisted. With the shear rate up to 0.3 s^{-1}, strings were formed, and then the strings coalesced with each other during shearing. Note that for the A20 blend, while strings coalesced into ribbons (the string width *W* was approximately 100 μm, $W>d$), some droplets broke up into smaller droplets (Ca = Ca_{cr}). It is clearly seen that strings were observed in all pure blends, whereas the ribbon-like structure was only observed in the A20 blend. After the cessation of shearing, the strings in A5 and A10 blends broke up into smaller droplets, while the widest ribbon-like strings in the A20 blend are relatively stable. The relaxation time (τ) of droplets or strings extends from 204 s for the A5 blend and 231 s for the A10 blend to 1152 s for the A20 blend. As compared with the bulk relaxation behavior of droplets in our previous work,[39] the τ was approximately 270 s for PA6 droplets ($2R = 80$ μm and AR = 10.8) in quiescent PS matrix (a bulk-like morphology, d=1600 μm). The τ for strings in the confined A20 blend is about quadruple times longer than that in bulk condition, which means that the stability of strings is improved in confined conditions.

Moreover, the effects of silica nanoparticles on the morphology development of ($PA6/SiO_2$)/PS 20/80 blends in confined shear flow were revealed in Figure 7. For A20 blends filled with different concentrations of silica nanoparticles, the initial morphology of the filled A20 blends was obviously refined as the nanoparticle content increased from 0 to 3 vol % (Figures 7a, e, and i) but notable coarsened droplets were

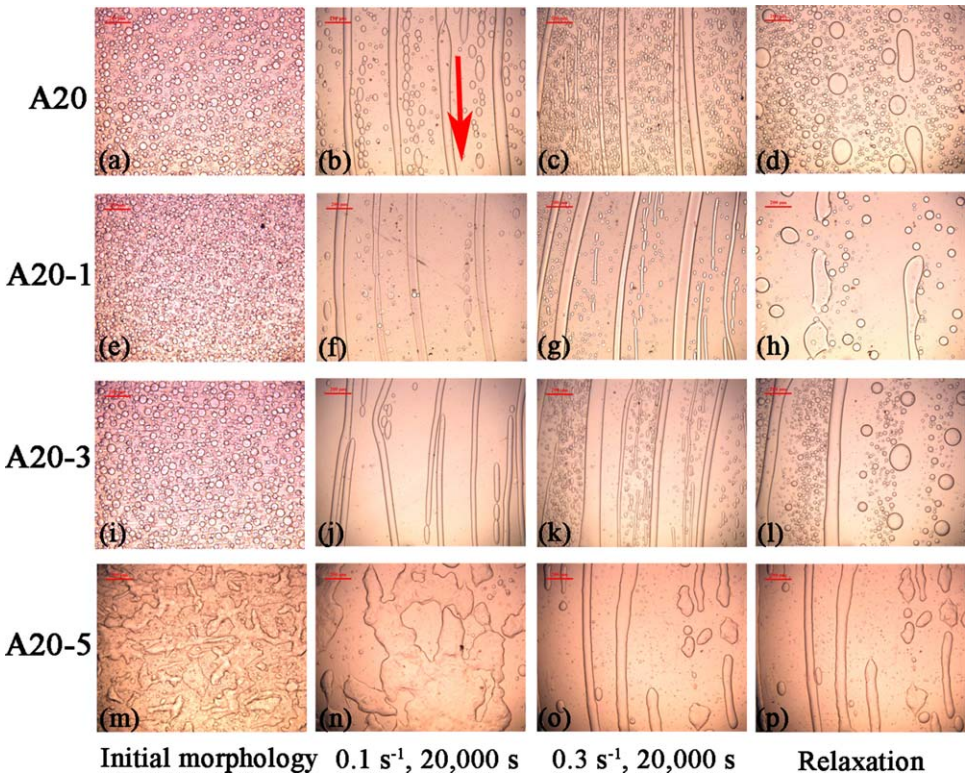

Figure 7. Morphology of ($PA6/SiO_2$)/PS 20/80 blends with different SiO_2 concentrations at 230°C with $d = 50$ μm before shearing (the first column), after shearing at 0.1 s^{-1} for 20,000 s (the second column), then shearing at 0.3 s^{-1} for another 20,000 s (the third column), and after relaxation for 1152 s (d), 4412 s (h), 4507 s (l), and 5555 s (p).

The red arrow denotes the flow direction, and the scale bar represents 200 μm. [Color figure can be viewed in the online issue, which is available at wileyonlinelibrary.com.]

observed in the A20-5 blend (Figure 7m). It is showed that as compared with the pure A20 blend, the confinement degree was decreased in the A20 blends filled with 1 and 3 vol % silica nanoparticles while it was increased in the A20 blends with 5 vol % silica nanoparticles. In confined shear flow, the morphology evolution of these blends exhibits obviously different microstructures, which differ from the morphology evolution of PA6/PS 20/80 blends under bulk conditions (a gap spacing of 300 micron).[41] After shearing in confined flow at 0.1 s^{-1} for 20,000 s, all droplets were in a single-layer and regularly aligned droplet chains, strings, and ribbon structure developed. The steady-state morphology of different A20 blends (Figures 7b, f, j, and n) displayed that in the presence of 1 vol % silica nanoparticles, ribbon-like strings were formed instead of the coexistence of ribbon-like droplets and pearl necklace structure in the pure A20 blend. As the nanoparticle content increased up to 3 vol %, more uniform strings were found, as shown in Figure 7j. For the A20-5 blend, a coarsened morphology was observed before shearing and became much coarser after shearing at 0.1 s^{-1} for 20,000 s (Figure 7n).

With the shear rates up to 0.3 s^{-1}, long ribbon-like strings and short droplet-like strings coexisted in A20, A20-1, and A20-3 blends. For the A20-5 blend, the coarsened morphology was elongated into strings. With increasing the nanoparticle content from 0 to 3 vol %, more strings or ribbons are observed and the string/ribbon width becomes bigger. It was found that the formation of strings or ribbons was promoted on the addition of silica nanoparticles although the initial morphology was refined at low nanoparticle contents. For the A20-5 blend, some of coarsened droplets could coalesce and elongate into strings/ribbons while others still existed and orientated perpendicularly to the shear direction. The orientation of droplets along the vorticity direction was provided that the droplet elasticity is sufficiently high.[44,45] In the A20-5 blend, some coarsened droplets orientated along the vorticity direction because of the 5 vol % nanoparticle-filled PA6 phase with high viscoelasticity, as shown in Figure 2.

After stopping shearing, relaxation behavior of the filled A20 blends was displayed in Figures 7d, h, l, and p. For A20 and A20-1 blends, the short strings can break up or retract into spherical droplets while the long strings or ribbons can break up but were difficult to retract even after relaxing 1152 s for A20 blend and 4412 s for A20-1 blend. Note that the ribbon-like strings in A20-3 and A20-5 blends were still stable even after relaxing for 4507 and 5555 s in A20-3 and A20-5 blends, respectively. It can be seen clearly that the selective filling of silica nanoparticles in dispersed droplets promoted the coalescence of droplets and thus increasing the droplet confinement, which facilitated the droplets to deform into strings when shearing at low shear rates in confined conditions and meanwhile to improve the stability of strings at high shear rates and after the stop of shearing.

Conclusions

Influences of silica nanoparticles on the morphology development of PA6/PS blends were systematically investigated in confined shear flow. Both the confinement and silica nanoparticles were found to promote the formation of PA6 droplet strings and improve the stability of droplets during confined shear flow. Aligned droplet chains were observed in confined blends at low shear rates while string-like structure was formed at high shear rates. Increasing the droplet or nanoparticle concentration will facilitate the coalescence of droplets and the formation of strings with improved stability. It was ascribed to the promoted coalescence of droplets induced by both the remarkably increased droplet viscoelasticity and the confinement, and the reduced interfacial tension by adding silica nanoparticles. Moreover, the experimental width and aspect ratio of droplets were compared with the model predictions. The experimental width of blends with low silica nanoparticle contents was in good agreement with the predictions of the M and mM models at small size of droplets and the MM model for all droplets. However, the experimental aspect ratio always showed a negative deviation to all model predictions, which might be ascribed to the omitted droplet orientation angle when using these models.

Acknowledgments

The authors are grateful to the financial support from the National Natural Science Foundation of China (51373109, 51421061, 51503133), the Fundamental Research Funds for the Central Universities (2013SCU04A02), Sichuan Youth Science and Technology Foundation (2015JQ0012), the Youth Start Funds of Sichuan University (2015SCU11030), the Innovation Team Program of Science & Technology Department of Sichuan Province (Grant 2013TD0013), and the State Key Laboratory of Polymer Materials Engineering of China (Grant No. sklpme2014-3-07).

Literature Cited

1. Migler KB. String formation in sheared polymer blends: coalescence, breakup, and finite size effects. *Phys Rev Lett*. 2001;86(6):1023–1026.
2. Yuan Z, Favis BD. Coarsening of immiscible co-continuous blends during quiescent annealing. *AIChE J*. 2005;51(1):271–280.
3. Perilla JE, Jana SC. Coalescence of immiscible polymer blends in chaotic mixers. *AIChE J*. 2005;51(10):2675–2685.
4. Tucker CL III, Moldenaers P. Microstructural evolution in polymer blends. *Annu Rev Fluid Mech*. 2002;34(1):177–210.
5. Tufano C, Peters G, Meijer H. Confined flow of polymer blends. *Langmuir*. 2008;24(9):4494–4505.
6. Pathak JA, Migler KB. Droplet-string deformation and stability during microconfined shear flow. *Langmuir*. 2003;19(21):8667–8674.
7. Van Puyvelde P, Vananroye A, Cardinaels R, Moldenaers P. Review on morphology development of immiscible blends in confined shear flow. *Polymer*. 2008;49(25):5363–5372.
8. De Bruyn P, Chen D, Moldenaers P, Cardinaels R. The effects of geometrical confinement and viscosity ratio on the coalescence of droplet pairs in shear flow. *J Rheol*. 2014;58(6):1955–1980.
9. Pathak JA, Davis MC, Hudson SD, Migler KB. Layered droplet microstructures in sheared emulsions: finite-size effects. *J Colloid Interface Sci*. 2002;255(2):391–402.
10. Vananroye A, Van Puyvelde P, Moldenaers P. Structure development in confined polymer blends: steady-state shear flow and relaxation. *Langmuir*. 2006;22(5):2273–2280.
11. Chen D, Cardinaels R, Moldenaers P. Effect of confinement on droplet coalescence in shear flow. *Langmuir*. 2009;25(22):12885–12893.
12. De Bruyn P, Cardinaels R, Moldenaers P. The effect of geometrical confinement on coalescence efficiency of droplet pairs in shear flow. *J Colloid Interface Sci*. 2013;409:183–192.
13. Vananroye A, Van Puyvelde P, Moldenaers P. Effect of confinement on droplet breakup in sheared emulsions. *Langmuir*. 2006;22(9):3972–3974.
14. Vananroye A, Cardinaels R, Van Puyvelde P, Moldenaers P. Effect of confinement and viscosity ratio on the dynamics of single droplets during transient shear flow. *J Rheol*. 2008;52(6):1459–1475.
15. Sibillo V, Pasquariello G, Simeone M, Cristini V, Guido S. Drop deformation in microconfined shear flow. *Phys Rev Lett*. 2006;97(5):54502.
16. Chen YP, Wang CY. Hydrodynamic interaction of two deformable drops in confined shear flow. *Phys Rev E*. 2014;90(3):033010.

17. Maffettone P, Minale M. Equation of change for ellipsoidal drops in viscous flow. *J Nonnewton Fluid Mech*. 1998;78(2-3):227–241.
18. Shapira M, Haber S. Low Reynolds number motion of a droplet in shear flow including wall effects. *Int J Multiphase Flow*. 1990;16(2):305–321.
19. Minale M. A phenomenological model for wall effects on the deformation of an ellipsoidal drop in viscous flow. *Rheol Acta*. 2008; 47(5):667–675.
20. Vananroye A, Van Puyvelde P, Moldenaers P. Effect of confinement on the steady-state behavior of single droplets during shear flow. *J Rheol*. 2007;51:139.
21. Minale M, Caserta S, Guido S. Microconfined shear deformation of a droplet in an equiviscous non-Newtonian immiscible fluid: experiments and modeling. *Langmuir*. 2009;26(1):126–132.
22. Cardinaels R, Verhulst K, Moldenaers P. Influence of confinement on the steady state behavior of single droplets in shear flow for immiscible blends with one viscoelastic component. *J Rheol*. 2009; 53(6):1403–1424.
23. Cardinaels R, Moldenaers P. Relaxation of fibrils in blends with one viscoelastic component: from bulk to confined conditions. *J Polym Sci B Polym Phys*. 2010;48(12):1372–1379.
24. Cardinaels R, Moldenaers P. Droplet relaxation in blends with one viscoelastic component: bulk and confined conditions. *Rheol Acta*. 2010;49(9):941–951.
25. Gupta A, Sbragaglia M. Deformation and breakup of viscoelastic droplets in confined shear flow. *Phys Rev E*. 2014;90(2):023305.
26. Cardinaels R, Vananroye A, Van Puyvelde P, Moldenaers P. Breakup criteria for confined droplets: effects of compatibilization and component viscoelasticity. *Macromol Mater Eng*. 2011;296(3-4):214–222.
27. Cardinaels R, Moldenaers P. Critical conditions and breakup of nonsquashed microconfined droplets: effects of fluid viscoelasticity. *Microfluid Nanofluid*. 2011;10(6):1153–1163.
28. Son Y, Martys NS, Hagedorn JG, Migler KB. Suppression of capillary instability of a polymeric thread via parallel plate confinement. *Macromolecules*. 2003;36(15):5825–5833.
29. Taguet A, Cassagnau P, Lopez-Cuesta J-M. Structuration, selective dispersion and compatibilizing effect of (nano) fillers in polymer blends. *Prog Polym Sci*. 2014;39(8):1526–1563.
30. Huang CW, Yu W. Role of block copolymer on the coarsening of morphology in polymer blend: effect of micelles. *AIChE J*. 2015; 61(1):285–295.
31. Li Q, Huang YJ, Xi ST, Yang Q, Li GX. Double emulsions of immiscible polymer blends stabilized by interfacially active nanoparticles. *AIChE J*. 2013;59(11):4373–4382.
32. Lepers JC, Favis BD. Interfacial tension reduction and coalescence suppression in compatibilized polymer blends. *AIChE J*. 1999;45(4): 887–895.
33. Zhang CL, Feng LF, Hoppe S, Hu GH. Compatibilizer-tracer: a powerful concept for polymer-blending processes. *AIChE J*. 2012; 58(6):1921–1928.
34. Vananroye A, Van Puyvelde P, Moldenaers P. Deformation and orientation of single droplets during shear flow: combined effects of confinement and compatibilization. *Rheol Acta*. 2011;50(3): 231–242.
35. Huang JR, Zhu YT, Jiang W, Cardinaels R, Moldenaers P, Shi D. Morphology control and stabilization in immiscible polypropylene and polyamide 6 blends with organoclay. *Int Polym Proc*. 2014; 29(4):522–534.
36. Taylor GI. The viscosity of a fluid containing small drops of another fluid. *Proc R Soc Lond A Math*. 1932;138(834):41–48.
37. Taylor GI. The formation of emulsions in definable fields of flow. *Proc R Soc Lond A Math*. 1934;146(858):501–523.
38. Choi SJ, Schowalter W. Rheological properties of nondilute suspensions of deformable particles. *Phys Fluids*. 1975;18:420.
39. Kong MQ, Huang YJ, Chen GL, Yang Q, Li GX. Retarded relaxation and breakup of deformed PA6 droplets filled with nanosilica in PS matrix during annealing. *Polymer*. 2011;52(22): 5231–5236.
40. De Bruijn R. Deformation and break-up of drops in simple shear flows. Ph.D. Thesis Technische Univ., Eindhoven, Netherlands, 1991.
41. Kong MQ, Huang YJ, Lv YD, Wang SH, Yang Q, Li GX. Flow-induced morphological instability in nanosilica-filled polyamide 6/ polystyrene blends. *Polymer*. 2014;55(16):4348–4357.
42. Feng J, Joseph D. The motion of solid particles suspended in viscoelastic liquids under torsional shear. *J Fluid Mech*. 1996;324:199–222.
43. Lyu SP, Bates FS, Macosko CW. Coalescence in polymer blends during shearing. *AIChE J*. 2000;46(2):229–238.
44. Hobbie E, Migler K. Vorticity elongation in polymeric emulsions. *Phys Rev Lett*. 1999;82:5393–5396.
45. Tanpaiboonkul P, Lerdwijitjarud W, Sirivat A, Larson RG. Transient and steady-state deformations and breakup of dispersed-phase droplets of immiscible polymer blends in steady shear flow. *Polymer*. 2007;48(13):3822–3835.

Manuscript received May 25, 2015, and revision received Aug. 23, 2015.